Available online at www.sciencedirect.com
ScienceDirect
Journal of Sound and Vibration 306 (2007) 691–711
JOURNAL OF SOUND AND VIBRATION
www.elsevier.com/locate/jsvi

# Frequency split and vibration localization in imperfect rings

Paolo Bisegna[a,*], Giovanni Caruso[b]

[a]*Department of Civil Engineering, University of Rome "Tor Vergata", 00133 Rome, Italy*
[b]*ITC-CNR, 00155 Rome, Italy*

Received 2 February 2007; received in revised form 7 June 2007; accepted 12 June 2007

**Abstract**

The dynamics of linearly elastic, imperfect rings vibrating in their own plane is considered in this paper. Imperfections are modeled as perturbations of the uniform linear mass density and bending stiffness of a perfect ring. A perturbation expansion and a spectral representation are employed, and a variational formulation of the vibration problem is obtained.

A linear theory is deduced by retaining only the leading-order terms in the variational formulation. The linear theory yields simple, closed-form expressions for the eigenfrequencies and the modal shapes, which are accurate when the imperfections are sufficiently small. An enhanced, nonlinear theory is also derived, which is accurate even when the ring imperfections are not small: in this case, an iterative solution procedure is developed.

The proposed theories are validated by considering some case-study problems and using the Ritz–Rayleigh solution as a benchmark.

Finally, the linear theory is applied to the frequency trimming problem of an imperfect ring. A simple, closed-form expression for the trimming masses is presented, valid for trimming any selected number of eigenmodes.


## 1. Introduction

Axisymmetric structures are commonly used in engineering applications, as turbine-bladed disks, satellite antennae, bells, stator–rotor assemblies in electrical machinery, vibrating ring gyroscopes, and so on. Due to the periodicity they possess, these structures exhibit degenerate pairs of spatially harmonic eigenmodes at the same frequency. It is well known that when structural irregularities are present, destroying the symmetry of the structure, the pairs of eigenfrequencies, coincident in the perfect symmetric case, split into two different values. In many cases, e.g., for vibrating ring gyroscopes [1,2,10] where a strong resonant coupling between two modes is required, the frequency split is a drawback effect and must be reduced with a correction procedure known as frequency trimming. Moreover, the eigenmodes of a structure with imperfections deviate from the sinusoidal shape: indeed, they present a local increase of the vibration amplitude, leading to an increase of the dynamical load acting on the vibrating structure. This phenomenon, known as vibration localization, may lead to fatigue failure [3,4]. For these reasons it is useful to have simple dynamical models able to take

*Corresponding author. Tel.: +39 62597097; fax: +39 672597005.
*E-mail addresses:* bisegna@uniroma2.it (P. Bisegna), g.caruso@ing.uniroma2.it (G. Caruso).

0022-460X/$ - see front matter © 2007 Elsevier Ltd. All rights reserved.
doi:10.1016/j.jsv.2007.06.027

into account the presence of imperfections and to predict the consequent frequency split and localization phenomenon.

The attention is focused here on the vibrations of linearly elastic imperfect rings. Many papers can be found in the literature dealing with a quantitative analysis of the frequency split occurring in these structures (e.g., Refs. [5,6] and the references cited therein). Diverse causes of imperfections have been considered by researchers and will be briefly summarized in what follows. In Ref. [7] a ring with variable cross-section was considered, and the Ritz–Rayleigh method was used to find out the eigenfrequencies; a closed-form expression for the lower natural frequency was obtained using a first-order approximation. In Ref. [5] a simple model for the frequency split of slightly imperfect rings was developed, based on the Ritz–Rayleigh method together with the simplifying assumption that the eigenmodes of the imperfect ring are still spatially harmonic. The imperfections were assumed to be generated by added masses or radial and torsional springs. Closed-form expressions for all the eigenfrequencies of the imperfect ring were obtained. An extension to the case of a distributed mass added to the ring was proposed in Ref. [8], and a study on the statistics of frequency splitting under various added random mass distributions was performed. In Ref. [6] in-plane profile variations were taken into account as a cause of frequency splitting. In Ref. [9] a ring comprised by an anisotropic material (crystalline silicon), implying a dependence of the Young modulus on the angular variable, was studied. According to the cited literature, while a great effort has been spent for the evaluation of the frequency split in imperfect rings, less attention has been devoted to the analysis of the modal shapes.

In this paper, a theory for the dynamics of linearly elastic imperfect rings vibrating in their own plane is proposed, yielding simple, closed-form expressions for both the eigenfrequencies and the modal shapes of the ring. Quite general imperfections are taken into account, by allowing the linear mass density and the in-plane bending stiffness of the ring to differ by a small perturbation, depending on the angular variable, from a uniform value relevant to a perfect ring. The Euler–Bernoulli theory is adopted, for the sake of simplicity, to build a dynamical model of the structure, under the assumption that the ring is axially inextensible. Generalizations of the present results to different kinematical models would be straightforward, if needed.

A perturbation expansion is performed: each eigenmode of the imperfect structure is represented by adding an unknown perturbation, depending on the angular variable, to the corresponding spatially harmonic eigenmode relevant to the perfect structure.

When only the leading-order terms are retained in the governing functional, a linear theory is obtained, yielding closed-form solutions for the modal eigenfrequencies and the modal shapes. An enhanced nonlinear theory is also derived by retaining higher-order terms, and an iterative procedure is proposed in order to find the corresponding solution.

For the sake of validation, some case-study problems are considered, and the results provided by the proposed theories are compared to the ones obtained by employing the Ritz–Rayleigh method. It turns out that the linear theory is accurate when imperfections are sufficiently small; for larger imperfections the enhanced theory may be used, and very accurate results are obtained after 2 or 3 iterations only.

Finally, the proposed theory is applied to the trimming problem of an imperfect ring. For the sake of comparison, the imperfect ring considered in Ref. [11] is studied and the first two elastic modes are trimmed by using the linear theory presented herein. This theory turns out to be a valid and simple tool for solving the trimming problem, since it yields, for any choice of modes to be trimmed, closed-form expressions of the trimming masses to be placed at arbitrary equally spaced positions. The quality of the achieved trimming is tested by evaluating the residual percentage mistuning between couples of trimmed eigenfrequencies, via the Ritz–Rayleigh method. Finally, a rule found in Ref. [12], concerning invalid combinations of masses and modes for single- or dual-mode trimming, is here generalized to multi-mode trimming.

## 2. Dynamical model of the ring

A model of the dynamical behavior of a circular ring is here derived, based on the classical Euler–Bernoulli theory. The ring has radius $R$ and is assumed to be linearly elastic. Let $\rho$ and $K$ denote, respectively, its linear

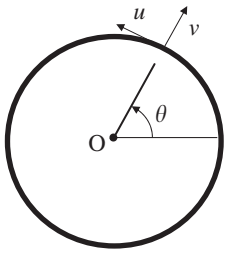


Fig. 1. Schematic representation of the ring.

mass density and in-plane bending stiffness. Due to the presence of imperfections, $\rho$ and $K$ are functions of the angular variable $\theta$. Let $u$ and $v$ be, respectively, the tangential and radial displacement of a point of the ring axis at the angular position $\theta$, as shown in Fig. 1.

It is assumed that the ring is axially inextensible, i.e. the circumferential strain $\varepsilon$ vanishes. Accordingly, the following condition prevails:

$$\varepsilon = \frac{1}{R}\left(\frac{\partial u}{\partial \theta} + v\right) = 0, \tag{1}$$

so that $v = -\partial u/\partial\theta$. The change of curvature is given by the well-known expression:

$$\Delta\chi = \frac{1}{R^2}\left(\frac{\partial u}{\partial \theta} - \frac{\partial^2 v}{\partial \theta^2}\right) = \frac{1}{R^2}\left(\frac{\partial u}{\partial \theta} + \frac{\partial^3 u}{\partial \theta^3}\right). \tag{2}$$

Accordingly, the Hamiltonian functional $\mathscr{H}$ describing the free vibrations of the ring is

$$\mathscr{H} = \frac{1}{2}\int_0^t \int_0^{2\pi} \rho\left[\left(\frac{\partial u}{\partial t}\right)^2 + \left(-\frac{\partial^2 u}{\partial\theta\partial t}\right)^2\right] R\,\mathrm{d}\theta\,\mathrm{d}t - \frac{1}{2}\int_0^t \int_0^{2\pi} \frac{K}{R^4}\left[\frac{\partial u}{\partial\theta} + \frac{\partial^3 u}{\partial\theta^3}\right]^2 R\,\mathrm{d}\theta\,\mathrm{d}t, \tag{3}$$

where $t$ is the time. The stationary condition for the functional (3) yields the dynamical equilibrium equation of the ring, which reads as follows:

$$R\frac{\partial^2}{\partial t^2}\left[\rho u - \frac{\partial}{\partial\theta}\left(\rho\frac{\partial u}{\partial\theta}\right)\right] - \left(\frac{\partial}{\partial\theta} + \frac{\partial^3}{\partial\theta^3}\right)\left[\frac{K}{R^3}\left(\frac{\partial u}{\partial\theta} + \frac{\partial^3 u}{\partial\theta^3}\right)\right] = 0. \tag{4}$$

Eq. (4) admits solutions harmonic in time, i.e. of the form:

$$u(\theta, t) = u(\theta)\mathrm{e}^{\mathrm{i}\omega t}, \tag{5}$$

where $\omega$ is the eigenfrequency, $\mathrm{i} = \sqrt{-1}$ is the imaginary unit, and, with a slight abuse of notation, $u(\theta)$ denotes the vibration amplitude. Accordingly, the dynamical equilibrium equation is recast as follows:

$$-\omega^2 R\left[\rho u - \frac{\partial}{\partial\theta}\left(\rho\frac{\partial u}{\partial\theta}\right)\right] - \left(\frac{\partial}{\partial\theta} + \frac{\partial^3}{\partial\theta^3}\right)\left[\frac{K}{R^3}\left(\frac{\partial u}{\partial\theta} + \frac{\partial^3 u}{\partial\theta^3}\right)\right] = 0. \tag{6}$$

For later usage, a weak version of Eq. (6) is presented. It is given by

$$-\omega^2\int_0^{2\pi}\rho\left(u\psi + \frac{\partial u}{\partial\theta}\frac{\partial\psi}{\partial\theta}\right)R\,\mathrm{d}\theta + \int_0^{2\pi}\frac{K}{R^4}\left(\frac{\partial u}{\partial\theta} + \frac{\partial^3 u}{\partial\theta^3}\right)\left(\frac{\partial\psi}{\partial\theta} + \frac{\partial^3\psi}{\partial\theta^3}\right)R\,\mathrm{d}\theta = 0 \tag{7}$$

for every $\psi$, test function belonging to the space $H^3_{\#}(\mathbf{R})$, composed of square integrable functions which are $2\pi$-periodic and have up to the third weak square integrable derivative with respect to $\theta$. The solution $u$ is searched for in the same function space $H^3_{\#}(\mathbf{R})$.

### 2.1. Perfect ring: degenerate eigenfrequencies and modal shapes

If the ring is perfect, then $\rho$ and $K$ do not depend on $\theta$, and are denoted by $\rho_o$ and $K_o$, respectively. Analogously, the function $u(\theta)$ is denoted by $u_o(\theta)$. Eq. (6) is simplified as follows:

$$-\omega^2 R\rho_o\left(u_o-\frac{\partial^2 u_o}{\partial\theta^2}\right)-\frac{K_o}{R^3}\left(\frac{\partial^2 u_o}{\partial\theta^2}+2\frac{\partial^4 u_o}{\partial\theta^4}+\frac{\partial^6 u_o}{\partial\theta^6}\right)=0. \tag{8}$$

For every natural number $n\in\mathbf{N}$, a solution of Eq. (8) is given by

$$u_{on}(\theta)=2A_{o,n}\cos(n\theta+\varphi_n)=U_{o,n}e^{in\theta}+U_{o,-n}e^{-in\theta}, \tag{9}$$

provided that the eigenfrequency $\omega$, denoted by $\omega_{on}$, is given by the following well-known formula:

$$\omega_{on}^2=\frac{K_o}{\rho_o R^4}\frac{n^2(1-n^2)^2}{1+n^2}. \tag{10}$$

Here

$$U_{o,n}=A_{o,n}e^{i\varphi_n},\quad U_{o,-n}=\overline{U}_{o,n}; \tag{11}$$

an overline denotes the complex conjugate, and $A_{o,n}\in\mathbf{R}^+$, $\varphi_n\in[0,2\pi)$ are arbitrary constants. In the literature, the eigenmode $u_{on}(\theta)$ is known as $n$th modal shape, $n$ is the number of its nodal diameters, and $\varphi_n$ is its phase orientation. It is recalled that for every $n\geqslant 1$, two independent eigenmodes $u_{on}$ exist, corresponding to the same eigenfrequency $\omega_{on}$: hence, they are referred to as degenerate eigenmodes. For $n=0$, only a single independent eigennode can be found. The eigenmodes relevant to $n=0$ and 1 correspond to rigid motions of the ring, and their eigenfrequencies are zero. In the following, the eigenmodes with $n\geqslant 2$ are considered. They have nonzero eigenfrequencies and imply deformations of the ring, so that they are known as elastic eigenmodes.

The modal shapes of the perfect ring corresponding to $n=2,3,4,5$ are reported in Fig. 6 with dashed/blue lines.

## 3. Imperfect ring: eigenfrequencies and modal shapes

It is well known that when even small imperfections are added to a perfect ring, thus destroying the rotational periodicity of the structure, the coinciding eigenfrequencies (10), relevant to couples of degenerate eigenmodes (9), split in two different values. Moreover, their corresponding eigenmodes deviate from the sinusoidal shape (9).

In this section, a model is presented, leading to analytical expressions of the eigenfrequencies and modal shapes of imperfect rings for quite general imperfection conditions.

### 3.1. Perturbation expansion

The presence of imperfections is accounted for as follows:

$$\rho=\rho_o+\delta\rho(\theta),\quad K=K_o+\delta K(\theta), \tag{12}$$

where $\delta\rho(\theta)$ and $\delta K(\theta)$ are, respectively, $2\pi$-periodic perturbations of the mass density $\rho_o$ and the bending stiffness $K_o$ of the perfect ring. Accordingly, the eigenmodes $u_n(\theta)$ and the corresponding eigenfrequencies $\omega_n$ of the imperfect ring are represented as

$$u_n(\theta)=u_{on}(\theta)+\delta u_n(\theta),\quad \omega_n=\omega_{on}+\delta\omega_n, \tag{13}$$

where $\delta u_n(\theta)$, here denoted as "harmonic distortion", is an unknown perturbation of the modal shape $u_{on}(\theta)$ of the perfect ring, accounting for the vibration localization, and $\delta\omega_n$ is the unknown shift of the corresponding modal eigenfrequency $\omega_{on}$.

By substituting the positions (12) and (13) into the weak formulation (7), the following variational equation is obtained:

$$-(\omega_{on}+\delta\omega_n)^2\int_0^{2\pi}(\rho_o+\delta\rho)\left[(u_{on}+\delta u_n)\psi+\frac{\partial(u_{on}+\delta u_n)}{\partial\theta}\frac{\partial\psi}{\partial\theta}\right]R\,\mathrm{d}\theta$$
$$+\int_0^{2\pi}\frac{K_o+\delta K}{R^4}\left(\frac{\partial}{\partial\theta}+\frac{\partial^3}{\partial\theta^3}\right)(u_{on}+\delta u_n)\left(\frac{\partial\psi}{\partial\theta}+\frac{\partial^3\psi}{\partial\theta^3}\right)R\,\mathrm{d}\theta=0 \tag{14}$$

for every $\psi\in H^3_{\#}(\mathbf{R})$. For each $n\geqslant 2$, two different solutions are expected, since the eigenmode degeneracy disappears due to imperfections: this is the frequency-splitting phenomenon. Hence, also the phase orientation $\varphi_n$ of the $n$th harmonic component of $u_n(\theta)$ must be regarded as an unknown quantity [5], which will be uniquely determined in what follows accounting for the presence of imperfections.

### 3.2. Linear theory

In order to develop closed-form expressions for the modal frequency shift $\delta\omega_n$ and the harmonic distortion $\delta u_n$, a linearized version of Eq. (14) is here derived. It is obtained by neglecting higher-order terms in Eq. (14):

$$\int_0^{2\pi}\left[-\omega_{on}^2\rho_o\left(\delta u_n\psi+\frac{\partial\delta u_n}{\partial\theta}\frac{\partial\psi}{\partial\theta}\right)+\frac{K_o}{R^4}\left(\frac{\partial\delta u_n}{\partial\theta}+\frac{\partial^3\delta u_n}{\partial\theta^3}\right)\left(\frac{\partial\psi}{\partial\theta}+\frac{\partial^3\psi}{\partial\theta^3}\right)\right]R\,\mathrm{d}\theta$$
$$=\int_0^{2\pi}\left[(\omega_{on}^2\delta\rho+2\rho_o\omega_{on}\delta\omega_n)\left(u_{on}\psi+\frac{\partial u_{on}}{\partial\theta}\frac{\partial\psi}{\partial\theta}\right)\right]R\,\mathrm{d}\theta$$
$$-\int_o^{2\pi}\left[\frac{\delta K}{R^4}\left(\frac{\partial u_{on}}{\partial\theta}+\frac{\partial^3 u_{on}}{\partial\theta^3}\right)\left(\frac{\partial\psi}{\partial\theta}+\frac{\partial^3\psi}{\partial\theta^3}\right)\right]R\,\mathrm{d}\theta \tag{15}$$

for every $\psi\in H^3_{\#}(\mathbf{R})$.

The mass–density perturbation $\delta\rho(\theta)$ and the bending–stiffness perturbation $\delta K(\theta)$ are represented by using Fourier series expansions:

$$\delta\rho(\theta)=\sum_{k=-\infty}^{+\infty}\{\delta\rho\}_k\,\mathrm{e}^{\mathrm{i}k\theta},\quad \delta K(\theta)=\sum_{k=-\infty}^{+\infty}\{\delta K\}_k\,\mathrm{e}^{\mathrm{i}k\theta}, \tag{16}$$

where $\{c\}$ is the vector containing the Fourier coefficients of a function $c(\theta)$, and $\{c\}_k$ is its $k$th component. Of course, it turns out that $\{c\}_{-k}=\overline{\{c\}}_k$. Also the unknown harmonic distortion $\delta u_n(\theta)$ is represented by using its Fourier series expansion:

$$\delta u_n(\theta)=\sum_{k=-\infty}^{+\infty}\{\delta u_n\}_k\,\mathrm{e}^{\mathrm{i}k\theta}. \tag{17}$$

Without loss of generality, we may assume that

$$\{\delta u_n\}_n=0, \tag{18}$$

since the phase orientation $\varphi_n$ is here assumed as an unknown quantity.

The Fourier series expansions (16) and (17) are substituted in Eq. (15). The test function $\psi$ is taken as follows:

$$\psi=\mathrm{e}^{-\mathrm{i}k\theta},\quad k\in\mathbf{N}. \tag{19}$$

After simple algebra, the following equation is obtained, for $k\in\mathbf{N}\backslash\{n\}$:

$$\frac{\{\delta u_n\}_k}{A_{o,n}}=\frac{1}{f_{kn}}\left[\frac{1+nk}{1+n^2}\mathrm{e}^{\mathrm{i}\varphi_n}\frac{\{\delta\rho\}_{-n+k}}{\rho_o}+\frac{1-nk}{1+n^2}\mathrm{e}^{-\mathrm{i}\varphi_n}\frac{\{\delta\rho\}_{n+k}}{\rho_o}\right]$$
$$-\frac{g_{kn}}{f_{kn}}\left[\mathrm{e}^{\mathrm{i}\varphi_n}\frac{\{\delta K\}_{-n+k}}{K_o}-\mathrm{e}^{-\mathrm{i}\varphi_n}\frac{\{\delta K\}_{n+k}}{K_o}\right], \tag{20}$$

where

$$g_{kn} = \frac{k(1-k^2)}{n(1-n^2)}, \quad h_{kn} = \frac{1+k^2}{1+n^2}, \quad f_{kn} = g_{kn}^2 - h_{kn}. \tag{21}$$

Eq. (20) yields the Fourier coefficients of the harmonic distortion $\delta u_n$. At the authors' knowledge, closed-form expressions for the eigenmodes $u_{on} + \delta u_n$ of the imperfect ring were not available in the literature.

On the other hand, the following equation is obtained for $k = n$:

$$0 = 2\mathrm{e}^{\mathrm{i}\varphi_n}\frac{\delta\omega_n}{\omega_{on}} + \left[\mathrm{e}^{\mathrm{i}\varphi_n}\frac{\{\delta\rho\}_0}{\rho_o} + \frac{1-n^2}{1+n^2}\mathrm{e}^{-\mathrm{i}\varphi_n}\frac{\{\delta\rho\}_{2n}}{\rho_o}\right] - \left[\mathrm{e}^{\mathrm{i}\varphi_n}\frac{\{\delta K\}_0}{K_o} - \mathrm{e}^{-\mathrm{i}\varphi_n}\frac{\{\delta K\}_{2n}}{K_o}\right]. \tag{22}$$

This equation yields:

$$\frac{\delta\omega_n}{\omega_{on}} = -\frac{1}{2}\frac{\{\delta\rho\}_0}{\rho_o} + \frac{1}{2}\frac{\{\delta K\}_0}{K_o} - \frac{1}{2}\mathrm{e}^{-2\mathrm{i}\varphi_n}\left[\frac{1-n^2}{1+n^2}\frac{\{\delta\rho\}_{2n}}{\rho_o} + \frac{\{\delta K\}_{2n}}{K_o}\right]. \tag{23}$$

Since the left-hand side and the first two terms at the right-hand side of the previous equation are real, also the third term at the right-hand side must be real. Thus, it follows that

$$\varphi_n = \frac{1}{2}\arg\left[\frac{1-n^2}{1+n^2}\frac{\{\delta\rho\}_{2n}}{\rho_o} + \frac{\{\delta K\}_{2n}}{K_o}\right] + l\frac{\pi}{2}, \quad l = 0, 1. \tag{24}$$

Hence

$$\frac{\delta\omega_n}{\omega_{on}} = -\frac{1}{2}\frac{\{\delta\rho\}_0}{\rho_o} + \frac{1}{2}\frac{\{\delta K\}_0}{K_o} - \frac{(-1)^l}{2}\left|\frac{1-n^2}{1+n^2}\frac{\{\delta\rho\}_{2n}}{\rho_o} + \frac{\{\delta K\}_{2n}}{K_o}\right|, \quad l = 0, 1, \tag{25}$$

where $|\cdot|$ denotes the modulus. As expected, it turns out that for each $n \geqslant 2$ (elastic modes) there are two sets of solutions of Eq. (15), denoted by $\{\delta\omega_{n,l}, \varphi_{n,l}, \delta u_{n,l}\}$, $l = 0, 1$. Hence, the frequency split (or mistuning) relevant to the mode $n$ turns out to be

$$\Delta\omega_n = (\omega_{on} + \delta\omega_{n,1}) - (\omega_{on} + \delta\omega_{n,0}) = \omega_{on}\left|\frac{1-n^2}{1+n^2}\frac{\{\delta\rho\}_{2n}}{\rho_o} + \frac{\{\delta K\}_{2n}}{K_o}\right|. \tag{26}$$

### 3.3. Enhanced theory

When the imperfections affecting the ring are not sufficiently small, the first-order closed-form solution given in the previous section may not be very accurate. Accordingly, it may be necessary to keep higher-order terms in (14), in order to improve the accuracy of the solution. To this end, the representation (16) of $\delta\rho$ and $\delta K$ and the representation (17) of $\delta u_n$ are substituted in Eq. (14), and all the terms appearing in the resulting equation are retained. Taking the test function $\psi$ defined in Eq. (19) and using Eq. (18), the following equation is obtained after simple algebra, for $k \in \mathbf{N}\backslash\{n\}$:

$$\begin{aligned}(g_{kn}^2 - h_{kn}\beta_n^2)\frac{\{\delta u_n\}_k}{A_{o,n}} = {} & \beta_n^2\left[\frac{1+nk}{1+n^2}\mathrm{e}^{\mathrm{i}\varphi_n}\frac{\{\delta\rho\}_{-n+k}}{\rho_o} + \frac{1-nk}{1+n^2}\mathrm{e}^{-\mathrm{i}\varphi_n}\frac{\{\delta\rho\}_{n+k}}{\rho_o}\right] \\ & + \frac{\beta_n^2}{1+n^2}\left[\left\{\frac{\{\delta\rho\}}{\rho_o} * \frac{\{\delta u_n\}}{A_{o,n}}\right\}_k - \mathrm{i}k\left\{\frac{\{\delta\rho\}}{\rho_o} * \frac{\{\partial\delta u_n/\partial\theta\}}{A_{o,n}}\right\}_k\right] \\ & - g_{kn}\left[\mathrm{e}^{\mathrm{i}\varphi_n}\frac{\{\delta K\}_{-n+k}}{K_o} - \mathrm{e}^{-\mathrm{i}\varphi_n}\frac{\{\delta K\}_{n+k}}{K_o}\right] \\ & + \frac{\mathrm{i}\,g_{kn}}{n(1-n^2)}\left\{\frac{\{\delta K\}}{K_o} * \frac{\{\partial\delta u_n/\partial\theta\} + \{\partial^3\delta u_n/\partial\theta^3\}}{A_{o,n}}\right\}_k,\end{aligned} \tag{27}$$

where $\beta_n = 1 + \delta\omega_n/\omega_{on}$ and $\{\{a\} * \{b\}\}_k$ denotes the $k$th component of the convolution product between the vectors $\{a\}$ and $\{b\}$, defined as follows:

$$\{\{a\} * \{b\}\}_k := \sum_{j=-\infty}^{+\infty} \{a\}_j \{b\}_{k-j}. \tag{28}$$

Moreover, $\{\partial c/\partial\theta\}_k = \mathrm{i}k\{c\}_k$, for a function $c(\theta)$. Taking $k = n$, the following equation is obtained:

$$\begin{aligned} 0 = {} & (\beta_n^2 - 1)\mathrm{e}^{\mathrm{i}\varphi_n} + \beta_n^2 \left[ \mathrm{e}^{\mathrm{i}\varphi_n} \frac{\{\delta\rho\}_0}{\rho_o} + \frac{1-n^2}{1+n^2} \mathrm{e}^{-\mathrm{i}\varphi_n} \frac{\{\delta\rho\}_{2n}}{\rho_o} \right] \\ & + \frac{\beta_n^2}{1+n^2} \left[ \left\{ \frac{\{\delta\rho\}}{\rho_o} * \frac{\{\delta u_n\}}{A_{o,n}} \right\}_n - \mathrm{i}n \left\{ \frac{\{\delta\rho\}}{\rho_o} * \frac{\{\partial\delta u_n/\partial\theta\}}{A_{o,n}} \right\}_n \right] \\ & - \left[ \mathrm{e}^{\mathrm{i}\varphi_n} \frac{\{\delta K\}_0}{K_o} - \mathrm{e}^{-\mathrm{i}\varphi_n} \frac{\{\delta K\}_{2n}}{K_o} \right] + \frac{\mathrm{i}}{n(1-n^2)} \left\{ \frac{\{\delta K\}}{K_o} * \frac{\{\partial\delta u_n/\partial\theta\} + \{\partial^3\delta u_n/\partial\theta^3\}}{A_{o,n}} \right\}_n . \end{aligned} \tag{29}$$

The system of Eqs. (27), (29) is nonlinear and fully coupled: thus, explicit solutions for the unknowns $\delta\omega_n$, $\varphi_n$ and $\{\delta u_n\}$ are not easily computed. Consequently, an iterative procedure is here adopted using, as initial guess, the values of $\delta\omega_{n,l}$, $\varphi_{n,l}$ and $\{\delta u_{n,l}\}$, $l = 0, 1$, given by the linear solution presented in Eqs. (25), (24) and (20), respectively. The iterative procedure is performed as follows. At the $j$th iteration, for $l = 0, 1$,

- $\delta\omega_n$ and $\varphi_n$ are updated by solving the first-order Taylor approximation of Eq. (29), after giving $\{\delta u_n\}$ the value obtained from the previous iteration.
- Then, the vector $\{\delta u_n\}$ is updated by using Eq. (27), after giving $\delta\omega_n$ and $\varphi_n$ the values computed above, and $\{\delta u_n\}$ appearing on the right-hand side of Eq. (27) the values obtained from the previous iteration.

Needless to say that the series at the right-hand side of Eq. (28), defining the convolution products appearing in Eqs. (27) and (29), must be truncated to a finite number of terms. However, since $\delta u \in H^3_{\#}(\mathbf{R})$, $\{\delta u\}_k$ rapidly decays as $|k| \to +\infty$ (in particular, $\sum_{k=-\infty}^{+\infty} |k^3\{\delta u\}_k|^2 < +\infty$), so that only few tens of terms are usually sufficient to obtain a satisfactory result. Numerical evidence reported in Section 5 shows the convergence and effectiveness of this computational scheme.

### 3.4. Numerical solution

In order to have a benchmark for validating the theories proposed in this paper, the Ritz–Rayleigh method is used to numerically solve the variational equation (7). To this end, the $n$th eigenfunction $u$ in Eq. (7) is represented as

$$u_n(\theta) = a_0 + \sum_{k=1}^{F} 2\, a_k \cos(k\theta) - \sum_{k=1}^{F} 2\, b_k \sin(k\theta), \tag{30}$$

where $F$ is a fixed natural number and, for each $n \in \mathbf{N}$, $a_0, a_k, b_k$, $k = 1 \ldots F$ are the real scalar unknowns of the resulting discrete problem, related to the complex Fourier coefficients of $u_n$ by the well-known equations: $a_0 = \{u_n\}_0$, $a_k = \mathrm{Re}(\{u_n\}_k)$ and $b_k = \mathrm{Im}(\{u_n\}_k)$.

For the sake of completeness, also a finite-element formulation has been derived, based on a two-node curvilinear-element discretization of the ring. The generic unknown modal shape $u_n$ is interpolated by means of its nodal values, and the nodal values of its first and second derivatives, by using the following shape functions:

$$1, \quad \theta, \quad \cos(\theta), \quad \sin(\theta), \quad \theta\cos(\theta), \quad \theta\sin(\theta), \tag{31}$$

which guarantee exact integration of constant and sinusoidal functions (i.e. exact reconstruction of rigid motions) and global continuity up to the second derivative, so that the interpolated functions are in the space $H^3_{\#}(\mathbf{R})$.

The two described approaches (Ritz–Rayleigh and finite-element methods) yield the same results, up to numerical round off. Accordingly, only results provided by the Ritz–Rayleigh approach will be reported in what follows.

## 4. Case-study problems

In this section two case-study problems of technological interest are presented, schematically shown in Fig. 2. Explicit solutions are derived for the split eigenfrequencies and eigenmodes of the imperfect ring, by employing the linear theory described in Section 3.2.

### 4.1. Lumped masses added to the ring

The imperfect ring shown in Fig. 2(a) is here considered. Its imperfection is due to $p$ lumped masses $m_j$ attached to the ring at angular positions $\theta = \Theta_j$, $j = 1 \dots p$. Accordingly, $\delta K(\theta) = 0$, whereas

$$\delta\rho(\theta) = \sum_{j=1}^{p} \frac{m_j}{R} \boldsymbol{\delta}_{\Theta_j}(\theta), \tag{32}$$

where $\boldsymbol{\delta}_{\Theta_j}$ denotes the Dirac delta function supported at $\Theta_j$. The Fourier coefficients of the mass density perturbation $\delta\rho$ are given by

$$\{\delta\rho\}_k = \sum_{j=1}^{p} \frac{m_j}{2\pi R} \mathrm{e}^{-\mathrm{i}k\Theta_j}. \tag{33}$$

Eq. (24) yields

$$\varphi_{n,l} = -\frac{1}{2}\arctan\frac{\sum_{j=1}^{p} m_j \sin 2n\Theta_j}{\sum_{j=1}^{p} m_j \cos 2n\Theta_j} + l\frac{\pi}{2}, \quad l = 0, 1, \tag{34}$$

whereas from Eq. (25) it turns out that

$$\frac{\delta\omega_{n,l}}{\omega_{on}} = -\frac{1}{2M_o}\left(\sum_{j=1}^{p} m_j - (-1)^l \frac{1-n^2}{1+n^2}\left|\sum_{j=1}^{p} m_j \mathrm{e}^{-\mathrm{i}2n\Theta_j}\right|\right), \quad l = 0, 1, \tag{35}$$

where $M_o = 2\pi R\rho_o$ is the mass of the perfect ring. Expression (34) of the phase orientation $\varphi_{n,l}$ is equivalent to expression (7) of $\psi_{n,l}$ derived in Ref. [11], by noting that $\psi_{n,l} = -\varphi_{n,l}/n$. The frequency shift in Eq. (35) coincides with the one given by the linearized version of Eqs. (11) and (12) of Ref. [11].

Finally, from Eq. (20), for $k \in \mathbf{N}\backslash\{n\}$, the Fourier coefficients of $\delta u_{n,l}$ are obtained:

$$\frac{\{\delta u_{n,l}\}_k}{A_{o,n}} = \frac{2}{M_o(1+n^2)f_{kn}} \sum_{j=1}^{p} \{m_j \mathrm{e}^{-\mathrm{i}k\Theta_j}[\cos(n\Theta_j + \varphi_{n,l}) + \mathrm{i}kn \sin(n\Theta_j + \varphi_{n,l})]\} \tag{36}$$

with $\varphi_{n,l}$ given in Eq. (34).

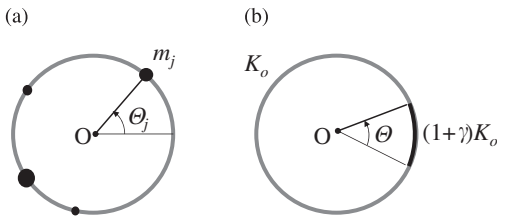


Fig. 2. (a) Lumped masses $m_j$ added to the ring at angular positions $\Theta_j$, $j = 1 \dots p$. (b) Massless stiffener applied to the ring, spanning the arc $[-\Theta/2, \Theta/2]$, locally increasing the bending stiffness by a quantity $\gamma K_o$.

In the special case of just one lumped mass $m$ added at the angle $\Theta$, Eqs. (34)–(36) reduce to

$$\begin{aligned} &\varphi_{n,0} = -n\Theta, && \varphi_{n,1} = -n\Theta + \frac{\pi}{2}, \\ &\frac{\delta\omega_{n,0}}{\omega_{on}} = -\frac{m}{M_o(1+n^2)}, && \frac{\delta\omega_{n,1}}{\omega_{on}} = -\frac{mn^2}{M_o(1+n^2)}, \\ &\frac{\{\delta u_{n,0}\}_k}{A_{o,n}} = \frac{2m\mathrm{e}^{-\mathrm{i}k\Theta}}{M_o(1+n^2)f_{kn}}, && \frac{\{\delta u_{n,1}\}_k}{A_{o,n}} = \frac{2mikn\mathrm{e}^{-\mathrm{i}k\Theta}}{M_o(1+n^2)f_{kn}}. \end{aligned} \tag{37}$$

### 4.2. Massless stiffener applied to the ring

The imperfect ring shown in Fig. 2(b) is here considered. The imperfection is due to a stiffener spanning the arc $[-\Theta/2, \Theta/2]$, having vanishing mass and constant bending stiffness, thus locally increasing the in-plane bending stiffness $K_o$ of the ring to the value $(1+\gamma)K_o$. As a consequence, $\delta\rho(\theta) = 0$, whereas

$$\delta K(\theta) = \gamma K_o \quad \text{for } \theta \in [-\Theta/2, \Theta/2]; \quad \delta K(\theta) = 0 \text{ otherwise.} \tag{38}$$

The Fourier coefficients of the perturbation $\delta K$ are given by

$$\{\delta K\}_k = \frac{\gamma K_o}{k\pi}\sin\frac{k\Theta}{2}. \tag{39}$$

Eq. (24) yields

$$\varphi_{n,l} = l\frac{\pi}{2}, \quad l = 0, 1, \tag{40}$$

whereas from Eq. (25) it is obtained:

$$\frac{\delta\omega_{n,l}}{\omega_{on}} = \frac{\gamma\Theta}{4\pi}\left[1 - (-1)^l\frac{\sin(n\Theta)}{n\Theta}\right], \quad l = 0, 1. \tag{41}$$

The Fourier coefficients of $\delta u_{n,l}$ are obtained from Eq. (20), for $k \in \mathbf{N}\backslash\{n\}$, and read as follows:

$$\frac{\{\delta u_{n,l}\}_k}{A_{o,n}} = -\frac{\mathrm{e}^{\mathrm{i}l\pi/2}\gamma\Theta}{2\pi}\frac{g_{kn}}{f_{kn}}\left\{\frac{\sin[(-n+k)\Theta/2]}{[(-n+k)\Theta/2]} - (-1)^l\frac{\sin[(n+k)\Theta/2]}{[(n+k)\Theta/2]}\right\}, \quad l = 0, 1. \tag{42}$$

## 5. Validation and numerical simulations

In this section, a validation of the models proposed in Sections 3.2 and 3.3 is performed by comparing their predictions to the ones supplied by the accurate Ritz–Rayleigh method described in Section 3.4.

For the sake of comparison, the perfect elastic ring considered in Refs. [5,11] is here chosen for the numerical simulations. The ring is comprised by a material with Young modulus $E = 206\,\mathrm{GPa}$, mass density $\mu = 7850\,\mathrm{kg/m^3}$ and Poisson's ratio $\nu = 0.3$. The ring radius is $R = 300\,\mathrm{mm}$, its thickness is $h = 5\,\mathrm{mm}$ and its axial length is $b = 100\,\mathrm{mm}$. Accordingly, the linear mass density $\rho_o = \mu bh$ is $3.925\,\mathrm{kg/m}$, the bending stiffness, assuming a plane strain condition, is $K_o = Eh^3/[12(1-\nu^2)] = 235.81\,\mathrm{N\,m^2}$ and the total mass is $M_o = 2\pi R\rho_o = 7.3984\,\mathrm{kg}$. The modal eigenfrequencies of the perfect ring are reported in Table 1, evaluated according to Eq. (10), and are coincident with the ones given in Table E1 of Ref. [11].

Table 1
Modal frequencies $f_{on} = \omega_{on}/(2\pi)$ of the perfect ring

| $n$ | 2 | 3 | 4 | 5 |
|---|---|---|---|---|
| $f_{on}$ (Hz) | 36.78 | 104.03 | 199.46 | 322.57 |

In order to perform the validation of the proposed models, the following cases of imperfection are considered:

(i) a single mass $m$ applied to the ring at $\theta = 0^\circ$ (this case is taken from Table 1 of Ref. [5]);
(ii) a stiffener spanning the arc $[-\Theta/2, \Theta/2]$, with $\Theta = 40^\circ$, applied to the ring, locally increasing the bending stiffness by a percentage $\gamma$;
(iii) three imperfection masses applied to the ring at the angles $\Theta_1 = 0^\circ, \Theta_2 = 20^\circ$ and $\Theta_3 = 70^\circ$. Their values are, respectively, $m_1 = 0.1\,\text{kg}$, $m_2 = 0.2\,\text{kg}$, $m_3 = 0.3\,\text{kg}$, globally amounting to about 8.1% of the perfect ring mass (this case is taken from Table 4 of Ref. [5] and Table 3 of Ref. [11]).

### 5.1. Frequency split

The frequency shifts and splits relevant to the above cases of imperfection are here computed by using the proposed theories and are compared to the ones obtained by using the Ritz–Rayleigh method. Moreover, for the cases (i) and (iii) of imperfection, results from Refs. [5,11] are also available. The following acronyms are introduced:

- LT refers to the linear theory presented in Section 3.2;
- ET-2 and ET-3 denote the enhanced theory reported in Section 3.3 (results obtained after 2 and 3 iterations, respectively);
- FT denotes the theory proposed in Refs. [5,11,12];
- RR denotes the Ritz–Rayleigh method described in Section 3.4.

Case (i) [resp., case (ii)] is analyzed in Fig. 3 and Table 2 [resp., Fig. 4 and Table 3]. Mode numbers $n = 2, 3, 4, 5$ are considered.

Fig. 3 [resp., Fig. 4] shows the frequency shifts $\delta\omega_{n,l}$ as a function of the ratio $m/M_o$ [resp., of the percentage $\gamma$]. Tables 2 and 3 report the relative error on the frequency shifts with respect to the RR solution, defined as follows:

$$\text{err}(\delta\omega_{n,l}) = \left| \frac{\delta\omega_{n,l} - \delta\omega_{n,l}^{\text{RR}}}{\delta\omega_{n,l}^{\text{RR}}} \right|. \tag{43}$$

As expected, in case (i) (Fig. 3) the frequency shifts are negative and decrease with increasing $m$, whereas in case (ii) (Fig. 4) they are positive and increase with increasing $\gamma$. The corresponding splits increase with increasing $m$ or $\gamma$. According to Eqs. (26), (33) and (39), they exhibit a slight [resp., marked] dependence on $n$ in case (i) [resp., case (ii)]. According to the LT model, the frequency splits and shifts linearly depend on the abscissa value (i.e., $m/M_o$ or $\gamma$).

It turns out that both the LT and FT models are in good agreement with the RR model for sufficiently small perturbations. Improved accuracy for larger perturbations is allowed by the enhanced ET model, even with only 2 or 3 iterations. This result can be quantitatively appreciated by looking at Tables 2 and 3. In particular, for $m/M_o = 1\%$ [resp., $\gamma = 4\%$] the LT and FT models supply a relative error of the order of some percent, whereas ET-2 guarantees an error below 0.2%, and ET-3 yields an error below 0.01%. Moreover, the ET-2 [resp., ET-3] model yields sufficiently [resp., very] accurate results even for $m/M_o = 5\%$ or $\gamma = 20\%$.

Finally, Table 4, relevant to case (iii) of imperfection, reports the modal frequencies $\omega_{n,l} = \omega_{on} + \delta\omega_{n,l}$ and the phase orientations $\varphi_{n,0}$ corresponding to mode numbers $n = 2, 3, 4, 5$ (according to LT and FT [5,11] methods, it turns out that $\varphi_{n,1} = \varphi_{n,0} + 90^\circ$). These results show that the LT and FT models are sufficiently accurate in predicting the eigenfrequencies even in this case; the phase orientations they predict are the same, whereas the modal frequencies are slightly different from each other. The enhanced theory with 3 iterations (ET-3), produces results which are almost coincident with the exact ones supplied by the RR method.

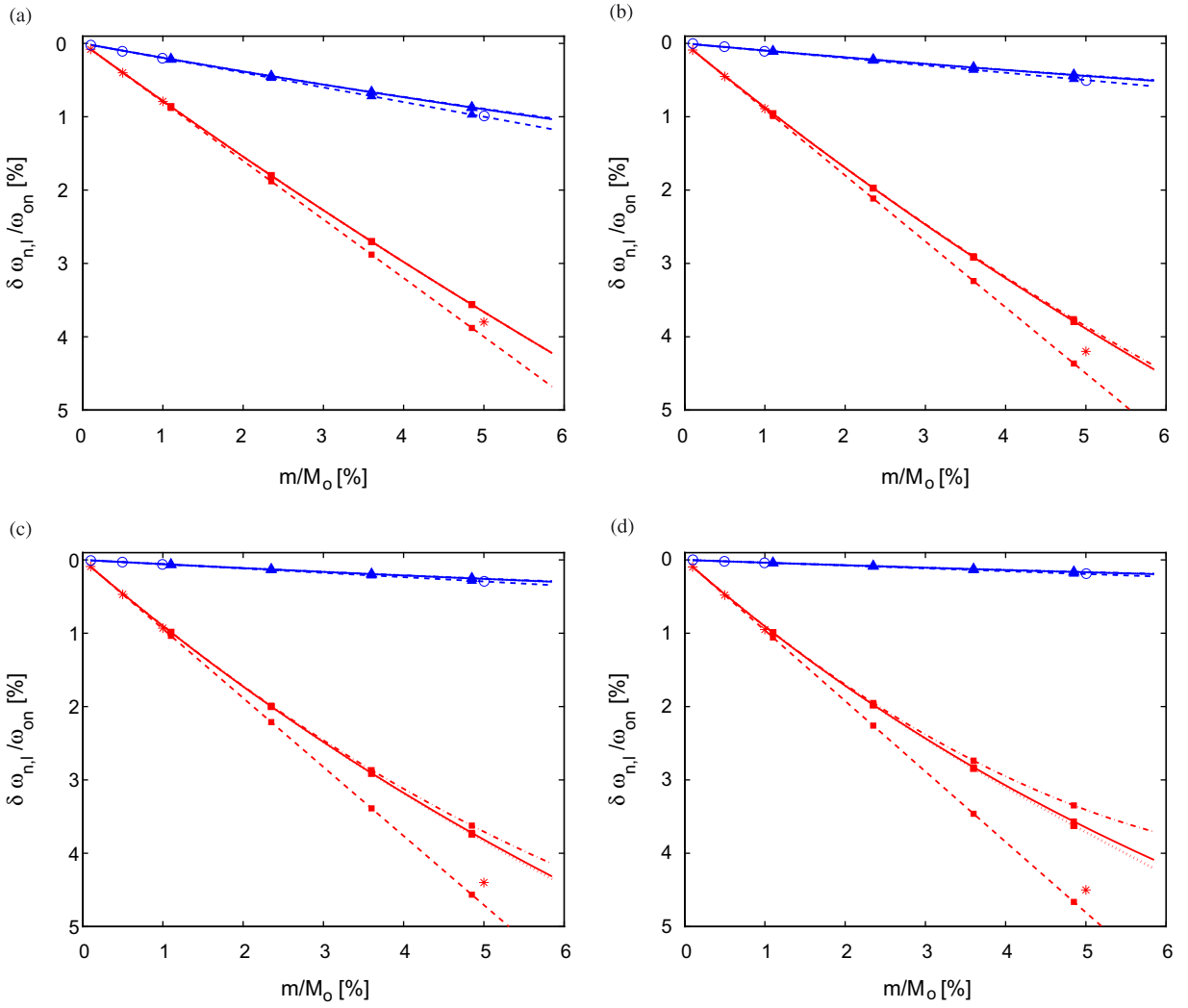


Fig. 3. Normalized frequency shift $\delta\omega_{n,l}/\omega_{on}$ (%) vs. normalized lumped mass $m/M_o$ (%) applied to the ring at $\theta = 0°$. Different theories adopted: - - LT, · - ET-2, · · · ET-3, — RR, ∗/∘ FT [5,11]. Lower- [resp., higher-] frequency split eigenmode $l = 0$ [resp., $l = 1$]: red/squares [resp., blue/triangles]. Eigenmodes: (a) $n = 2$; (b) $n = 3$; (c) $n = 4$; (d) $n = 5$.

Table 2
Relative error err($\delta\omega_{n,l}$) (%) on the frequency shift with respect to the RR solution

| $m/M_o$ (%) | Theory | $n = 2$ | | $n = 3$ | | $n = 4$ | | $n = 5$ | |
|---|---|---|---|---|---|---|---|---|---|
| 1% | LT | 1.83 | 2.27 | 3.04 | 2.55 | 4.45 | 2.71 | 5.96 | 2.81 |
| | FT [5] | 0.55 | 2.26 | 1.89 | 2.55 | 3.21 | 4.76 | 4.69 | 1.57 |
| | ET–2 | $2 \times 10^{-5}$ | 0.039 | 0.029 | 0.058 | 0.094 | 0.069 | 0.21 | 0.075 |
| | ET–3 | $1 \times 10^{-7}$ | $8 \times 10^{-4}$ | $4.9 \times 10^{-4}$ | 0.0014 | 0.0029 | 0.0018 | 0.0097 | 0.0021 |
| 5% | LT | 9.22 | 11.3 | 15.6 | 12.7 | 23.3 | 13.6 | 31.7 | 14.0 |
| | FT [5] | 3.76 | 10.2 | 7.95 | 12.7 | 15.3 | 12.0 | 23.3 | 12.7 |
| | ET–2 | 0.0015 | 0.96 | 0.83 | 1.44 | 2.84 | 1.72 | 6.59 | 1.89 |
| | ET–3 | $1 \times 10^{-4}$ | 0.09 | 0.08 | 0.17 | 0.49 | 0.22 | 1.71 | 0.26 |

Imperfection due to a lumped mass $m$, according to case (i). Eigenmodes $n = 2, 3, 4, 5$: split eigenmode $l = 0$ [resp., $l = 1$] on the left [resp., on the right]. Different theories adopted (see text).

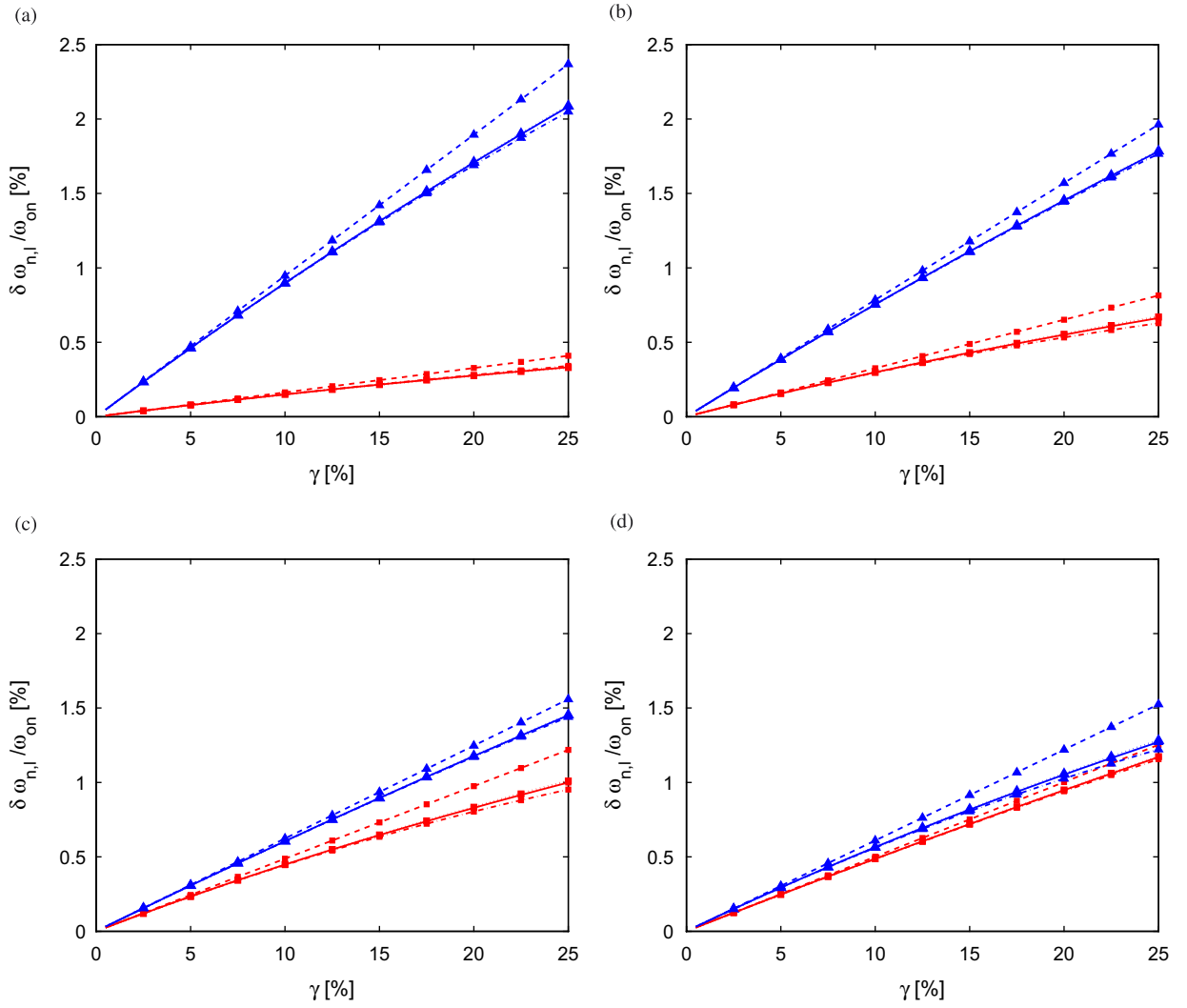


Fig. 4. Normalized frequency shift $\delta\omega_{n,l}/\omega_{on}$ (%) vs. percentage bending-stiffness increase $\gamma$ (%) due to a stiffener spanning the arc $[-20^\circ, 20^\circ]$. Different theories adopted: -- LT, ·· ET-2, ··· ET-3, — RR. Lower- [resp., higher-] frequency split eigenmode $l = 0$ [resp., $l = 1$]: red/squares [resp., blue/triangles]. Eigenmodes: (a) $n = 2$; (b) $n = 3$; (c) $n = 4$; (d) $n = 5$.

Table 3
Relative error err($\delta\omega_{n,l}$) (%) on the frequency shift with respect to the RR solution

| $\gamma$ (%) | Theory | $n = 2$ | | $n = 3$ | | $n = 4$ | | $n = 5$ | |
|---|---|---|---|---|---|---|---|---|---|
| 4% | LT | 3.72 | 2.20 | 3.68 | 1.62 | 3.52 | 1.21 | 1.20 | 3.18 |
| | ET–2 | 0.035 | 0.041 | 0.13 | 0.024 | 0.12 | 0.02 | 0.034 | 0.098 |
| | ET–3 | 0.0012 | $8.8 \times 10^{-4}$ | 0.0051 | $4.6 \times 10^{-7}$ | 0.0043 | $5.7 \times 10^{-4}$ | 0.0013 | 0.0032 |
| 20% | LT | 18.5 | 11.0 | 18.3 | 8.10 | 17.6 | 5.97 | 5.73 | 16.0 |
| | ET–2 | 1.52 | 1.02 | 3.34 | 0.59 | 3.02 | 0.47 | 0.78 | 2.47 |
| | ET–3 | 0.27 | 0.11 | 0.63 | 0.057 | 0.55 | 0.067 | 0.15 | 0.41 |

Imperfection due to a massless stiffener increasing the bending stiffness of $\gamma K_o$, according to case (ii). Eigenmodes $n = 2, 3, 4, 5$: split eigenmode $l = 0$ [resp., $l = 1$] on the left [resp., on the right]. Different theories adopted (see text).

Table 4
Phase orientations $\varphi_{n,0}$ (deg) and modal frequencies $f_{n,l} = \omega_{n,l}/(2\pi)$ (Hz), relevant to the imperfect ring of case (iii)

| Theory | $n=2$ | | | $n=3$ | | | $n=4$ | | | $n=5$ | | |
|---|---|---|---|---|---|---|---|---|---|---|---|---|
| | $\varphi_{n,0}$ | $f_{n,l}$ | | $\varphi_{n,0}$ | $f_{n,l}$ | | $\varphi_{n,0}$ | $f_{n,l}$ | | $\varphi_{n,0}$ | $f_{n,l}$ | |
| LT | −6.95 | 34.973 | 35.603 | 11.82 | 97.232 | 102.386 | 23.16 | 186.96 | 195.79 | −4.14 | 304.29 | 314.70 |
| FT [5,11] | −6.95 | 35.096 | 35.656 | 11.82 | 97.832 | 102.423 | 23.16 | 188.02 | 195.89 | −4.14 | 305.71 | 314.97 |
| ET–2 | −6.75 | 35.138 | 35.733 | 12.13 | 98.284 | 102.504 | 24.30 | 189.83 | 195.97 | −2.76 | 308.89 | 315.46 |
| ET–3 | −6.73 | 35.139 | 35.727 | 12.14 | 98.203 | 102.490 | 24.30 | 189.21 | 195.98 | −2.97 | 307.53 | 315.29 |
| RR | −6.74 | 35.139 | 35.728 | 12.14 | 98.216 | 102.492 | 24.29 | 189.35 | 195.98 | −2.95 | 307.97 | 315.31 |

Eigenmodes $n = 2, 3, 4, 5$: $f_{n,0}$ [resp., $f_{n,1}$] on the left [resp., on the right]. Different theories adopted (see text).

Table 5
Relative error $\mathrm{err}(u_{n,l})$ (%) on the eigenmodes

| $m/M_o$ (%) | $n=2$ | | $n=3$ | | $n=4$ | | $n=5$ | |
|---|---|---|---|---|---|---|---|---|
| 1% | 0.013 | 0.033 | 0.067 | 0.042 | 0.18 | 0.046 | 0.35 | 0.048 |
| 5% | 0.33 | 0.77 | 1.61 | 0.96 | 4.1 | 1.04 | 7.58 | 1.09 |

Imperfection due to a lumped mass $m$, according to case (i). Eigenmodes $n = 2, 3, 4, 5$: split eigenmode $l = 0$ [resp., $l = 1$] on the left [resp., on the right]. LT model adopted in the computations.

### 5.2. Modal shapes

The ability of the proposed theories to evaluate the modal shapes of an imperfect ring is here investigated. To this end, the imperfection cases (i) and (ii) are considered, and the following relative error measure is introduced:

$$\mathrm{err}(u_{n,l}) = \frac{\|u_{n,l} - u_{n,l}^{\mathrm{RR}}\|_2}{\|u_{n,l}^{\mathrm{RR}}\|_2} = \sqrt{\frac{\sum_{k=-\infty}^{+\infty} |\{u_{n,l}\}_k - \{u_{n,l}^{\mathrm{RR}}\}_k|^2}{\sum_{k=-\infty}^{+\infty} |\{u_{n,l}^{\mathrm{RR}}\}_k|^2}}, \tag{44}$$

where $\|\cdot\|_2$ denotes the $L^2$ norm over $[0, 2\pi)$ and the modal shape $u_{n,l}^{\mathrm{RR}}$ supplied by the RR method is used as a benchmark.

In Table 5 [resp., Table 6] the relative error relevant to mode numbers $n = 2, 3, 4, 5$ is reported, for two different values of $m/M_o$ [resp., $\gamma$]. They are computed using the LT model; the ET model supplies vanishing errors (not reported), while no data are available for the FT model, based on the assumption that modal shapes are unaffected by imperfections. In the considered cases, the LT model appears to be sufficiently accurate for estimating the modal shapes of imperfect rings.

In order to study the vibration localization phenomenon due to the presence of imperfections, the following total harmonic distortion (THD) index is introduced for each split eigenmode:

$$\mathrm{THD} = \frac{\|\delta u_{n,l}\|_2}{\|u_{on}\|_2} = \sqrt{\frac{\sum_{k=-\infty}^{+\infty} |\{\delta u_{n,l}\}_k|^2}{2A_{on}^2}}. \tag{45}$$

This index measures the contribution of harmonics different from the fundamental one $u_{on}$ to the modal shape $u_{n,l}$ of the imperfect ring.

In Fig. 5 the THD index, evaluated using the LT model for mode numbers $n = 2, 3, 4, 5$, is reported: panel (a) refers to case (i) (lumped added mass), whereas panel (b) refers to case (ii) (added stiffener). Very similar results, not reported, are obtained by using the ET or RR model. It turns out that imperfections imply an appreciable harmonic distorsion, increasing with the increase of the mode number $n$. As an example, in the

Table 6
Relative error err($u_{n,l}$) (%) on the eigenmodes

| $\gamma$ (%) | $n=2$ | | $n=3$ | | $n=4$ | | $n=5$ | |
|---|---|---|---|---|---|---|---|---|
| 4% | 0.15 | 0.14 | 0.32 | 0.31 | 0.27 | 0.25 | 0.22 | 0.20 |
| 20% | 0.79 | 0.65 | 1.71 | 1.36 | 1.54 | 1.12 | 1.17 | 0.94 |

Imperfection due to a massless stiffener increasing the bending stiffness of $\gamma K_o$, according to case (ii). Eigenmodes $n=2,3,4,5$: split eigenmode $l=0$ [resp., $l=1$] on the left [resp., on the right]. LT model adopted in the computations.

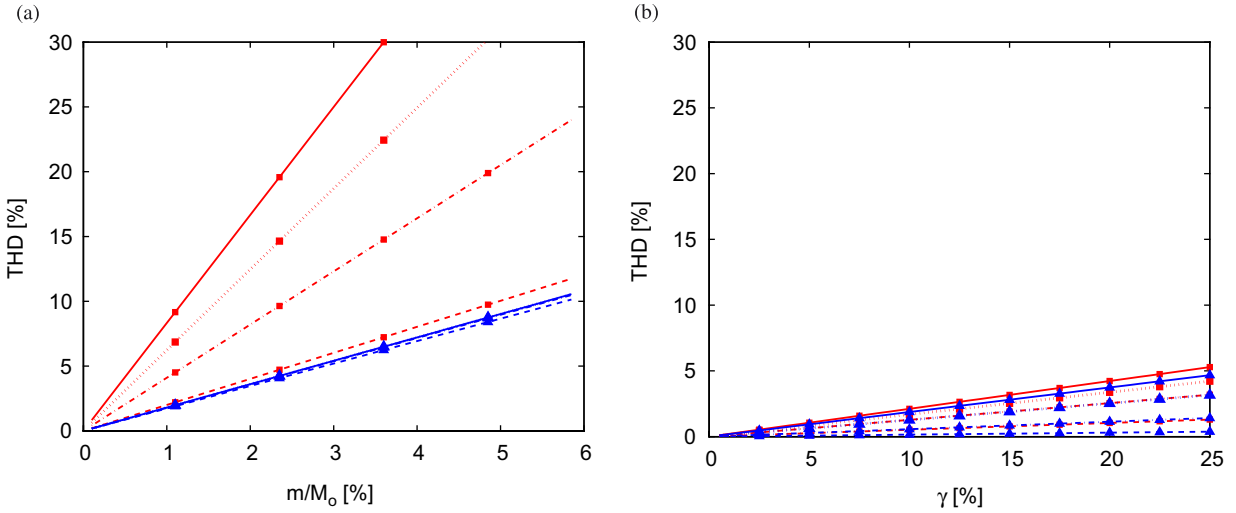


Fig. 5. Total harmonic distortion coefficient THD (%) vs. (a) normalized lumped mass $m/M_o$ (%) applied to the ring at $\theta=0$, or vs. (b) percentage bending-stiffness increase $\gamma$ (%) due to a stiffener spanning the angle $[-20°, 20°]$. Lower- [resp., higher-] frequency split eigenmode $l=0$ [resp., $l=1$]: red/squares [resp., blue/triangles]. Eigenmodes: - - $n=2$, · · $n=3$, ··· $n=4$, — $n=5$. LT theory adopted in the computations.

case of lumped added mass, the THD index becomes quite large for the lower-frequency split eigenmode ($l=0$), being in excess of 30% for mode number $n=5$ and for a mass ratio $m/M_o>4\%$.

Finally, in Fig. 6 the modal shapes $u_{n,l}$ of an imperfect ring, evaluated by using the LT model (continuous/red lines) and the RR model (black crosses), are compared and superimposed to the corresponding modes of the perfect ring (dashed/blue lines). The ring is made imperfect according to case (iii). The presence of harmonics different from the fundamental one is appreciable, and become significant for higher mode numbers $n$. The related localization phenomenon is emphasized in Fig. 7, where the perturbations $\delta u_{n,l}=u_{n,l}-u_{on}$ of the modal shapes are reported, with respect to a circular reference. A quantitative measure of this phenomenon is given in Tables 7 and 8. Table 7 shows that the THD ranges from 10% to 30% when the mode number $n$ ranges from 2 to 5. Moreover, a satisfactory agreement between the LT and RR models can be observed even in the present case, where the imperfection masses globally amount to about 8.1% of the perfect ring mass. Table 8 shows what the harmonic content of the distortion $\delta u_{n,l}$ is: it turns out that a significant contribution is due to the harmonics $\{\delta u_{n,l}\}_k$ for $0\leqslant k\leqslant n-1$.

## 6. Trimming

Let an imperfect ring be assigned. As it was recalled above, its eigenmodes are not, in general, degenerate, and frequency splits do occur. The goal is to perform a trimming procedure, aimed to eliminate such splits, at least for the eigenmodes $n\in\mathcal{N}$, where $\mathcal{N}$ is a given set of mode numbers.

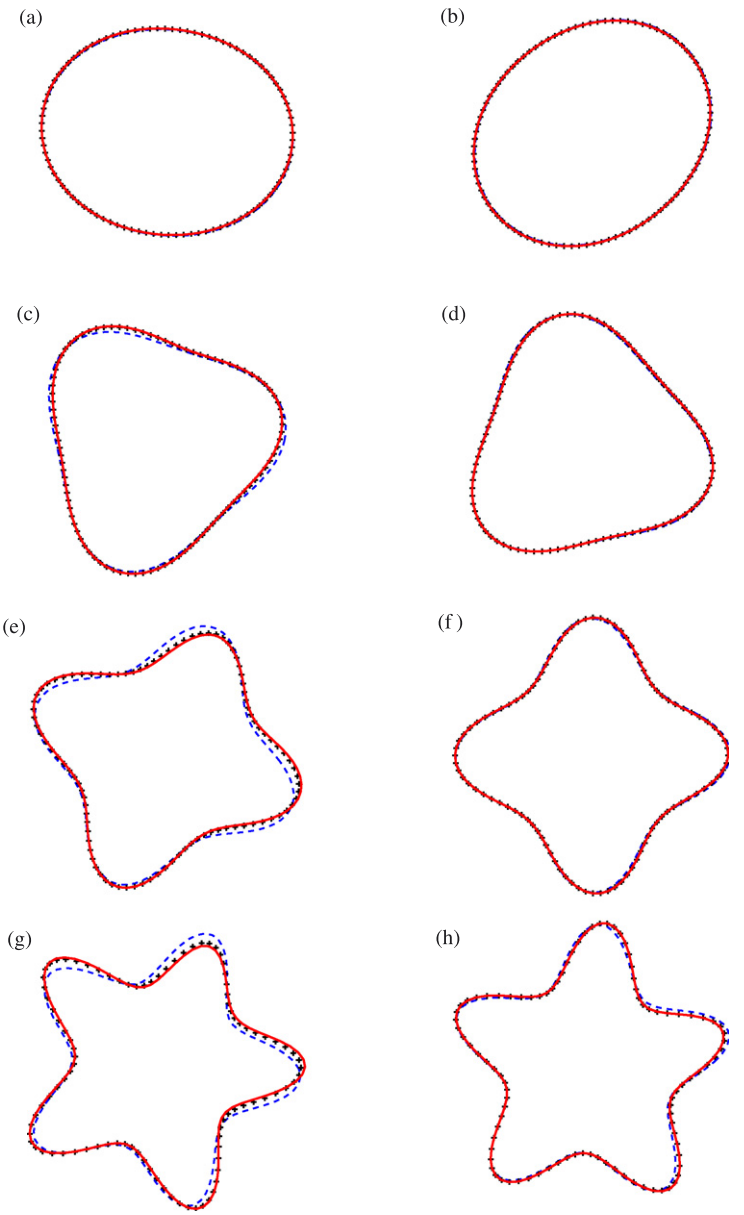


Fig. 6. Modal shapes $u_{n,l}(\theta)$ of a perfect ring (- -/blue) and imperfect ring (LT model: —/red; exact RR solution: +/black). Imperfection due to three lumped masses, according to case (iii). Eigenmodes: (a) $n=2$, $l=0$; (b) $n=2$, $l=1$; (c) $n=3$, $l=0$; (d) $n=3$, $l=1$; (e) $n=4$, $l=0$; (f) $n=4$, $l=1$; (g) $n=5$, $l=0$; (h) $n=5$, $l=1$.

This goal may be achieved by adding a suitable continuous mass distribution $\delta\rho_{\mathrm{tr}}(\theta)$ to the ring. Alternatively, following Ref. [12], a suitable number $N$ of point masses $\{m_{l,\mathrm{tr}}\}_{l=1\ldots N}$ to be determined may be added to the ring at locations $\{\Theta_{l,\mathrm{tr}}\}_{l=1\ldots N}$ which, in turn, may be preselected or free (i.e., *a priori* unknown).

In this section, very simple closed-form formulas to achieve frequency trimming on the eigenmodes $n \in \mathcal{N}$ are presented. In particular, these formulas yield the values of the point masses $\{m_{l,\mathrm{tr}}\}$, to be applied to the ring at the preselected locations $\{\Theta_{l,\mathrm{tr}}\}$, or alternatively the mass distribution $\delta\rho_{\mathrm{tr}}(\theta)$ needed for trimming. The argument relies on the linear theory proposed in Section 3.2. The quality of the trimming achieved is evaluated by computing the exact eigenfrequencies of the trimmed ring via the Ritz–Rayleigh method.

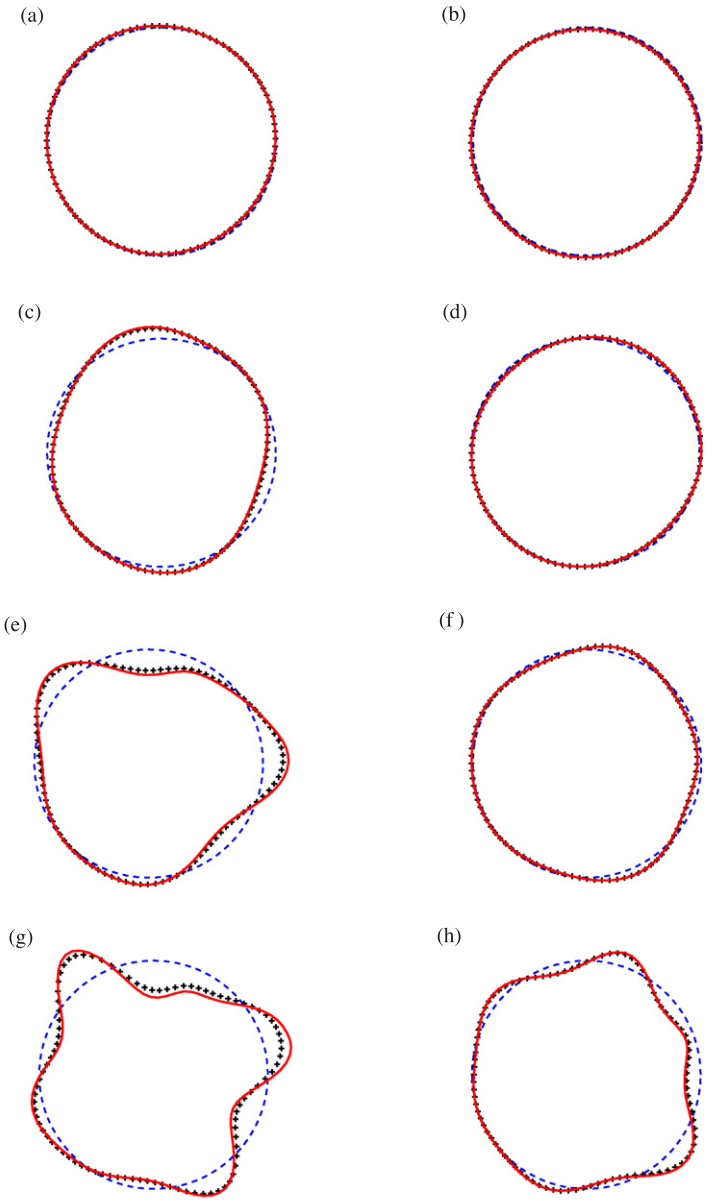


Fig. 7. Perturbation $\delta u_{n,l}(\theta) = u_{n,l}(\theta) - u_{on}(\theta)$ of the modal shapes of an imperfect ring (LT model: —/red; exact RR solution: +/black; reference: - -/blue). Imperfection due to three lumped masses, according to case (iii). Amplification of the harmonic distorsion: 2 times with respect to Fig. 6. Eigenmodes: (a) $n = 2$, $l = 0$; (b) $n = 2$, $l = 1$; (c) $n = 3$, $l = 0$; (d) $n = 3$, $l = 1$; (e) $n = 4$, $l = 0$; (f) $n = 4$, $l = 1$; (g) $n = 5$, $l = 0$; (h) $n = 5$, $l = 1$.

Of course, in order to achieve a trimming, it is necessary, as a first step, to experimentally characterize the imperfect ring. The experimental measurements yield the imperfect ring eigenfrequencies $\omega_{n,0}$ and $\omega_{n,1}$, whose difference

$$\Delta\omega_{n,\mathrm{exp}} = \omega_{n,1} - \omega_{n,0} = \delta\omega_{n,1} - \delta\omega_{n,0} \tag{46}$$

is the modal split (or mistuning). Moreover, they yield the phase orientations of the eigenmodes $n \in \mathscr{N}$. Let $\varphi_{n,\mathrm{exp}}$ be the phase orientation relevant to the lower-frequency (i.e., $l = 0$) split eigenmode.

Table 7
Total harmonic distortion coefficient THD (%) relevant to case (iii)

| | $n=2$ | | $n=3$ | | $n=4$ | | $n=5$ | |
|---|---|---|---|---|---|---|---|---|
| LT | 12.05 | 10.98 | 21.11 | 8.13 | 29.48 | 9.27 | 33.66 | 20.99 |
| RR | 10.65 | 10.18 | 18.84 | 7.08 | 24.22 | 9.35 | 28.29 | 18.90 |

Eigenmodes $n=2,3,4,5$: split eigenmode $l=0$ [resp., $l=1$] on the left [resp., on the right]. LT and RR models adopted in the computations.

Table 8
Harmonic content $|\{u_{n,l}\}_k|$, $k=0\ldots9$, of the eigenmode $u_{n,l}$ relevant to case (iii)

| $k$ | $n=2$ | | $n=3$ | | $n=4$ | | $n=5$ | |
|---|---|---|---|---|---|---|---|---|
| 0 | 0.0859 | 0.0147 | 0.0145 | 0.0095 | 0.0492 | 0.0289 | 0.0711 | 0.0774 |
| 1 | 0.1035 | 0.1093 | 0.1151 | 0.0596 | 0.1004 | 0.0572 | 0.1572 | 0.1437 |
| 2 | **1.0000** | **1.0000** | 0.1732 | 0.0544 | 0.1657 | 0.0430 | 0.1234 | 0.0921 |
| 3 | 0.0108 | 0.0034 | **1.0000** | **1.0000** | 0.2126 | 0.0515 | 0.1430 | 0.0629 |
| 4 | 0.0017 | 0.0002 | 0.0343 | 0.0070 | **1.0000** | **1.0000** | 0.2144 | 0.0790 |
| 5 | 0.0003 | 0.0002 | 0.0061 | 0.0015 | 0.0537 | 0.0196 | **1.0000** | **1.0000** |
| 6 | 0.0001 | 0.0001 | 0.0012 | 0.0008 | 0.0101 | 0.0047 | 0.0651 | 0.0397 |
| 7 | 0.0001 | 0.0001 | 0.0005 | 0.0005 | 0.0017 | 0.0011 | 0.0101 | 0.0126 |
| 8 | 0.0000 | 0.0000 | 0.0004 | 0.0003 | 0.0015 | 0.0002 | 0.0043 | 0.0049 |
| 9 | 0.0000 | 0.0000 | 0.0003 | 0.0001 | 0.0015 | 0.0003 | 0.0050 | 0.0020 |

Normalization: $A_{o,n}=|\{u_{n,l}\}_n|=1$. Eigenmodes $n=2,3,4,5$: split eigenmode $l=0$ [resp., $l=1$] on the left [resp., on the right]. LT model adopted in the computations.

Following Ref. [5], the trimming procedure here adopted hinges on determining a continuous mass distribution $\delta\rho_{\rm exp}(\theta)$, which, if added to a perfect reference ring $\mathscr{R}_{\rm ref}$, would produce modal mistunings $\omega_{n,1}-\omega_{n,0}$ and phase orientations $\varphi_{n,0}$ on the eigenmodes $n\in\mathscr{N}$, which coincide with the corresponding measured quantities $\Delta\omega_{n,\rm exp}$ and $\varphi_{n,\rm exp}$, respectively. Hence, the mass distribution $\delta\rho_{\rm exp}(\theta)$, according to Eqs. (26) and (24), must satisfy the equations:

$$\Delta\omega_{n,\rm exp}=\omega_{on}\left|\frac{1-n^2}{1+n^2}\frac{\{\delta\rho_{\rm exp}\}_{2n}}{\rho_o}\right|,\quad n\in\mathscr{N} \tag{47}$$

and

$$\varphi_{n,\rm exp}=\frac{1}{2}\arg\left[\frac{1-n^2}{1+n^2}\frac{\{\delta\rho_{\rm exp}\}_{2n}}{\rho_o}\right],\quad n\in\mathscr{N}, \tag{48}$$

which yield:

$$\{\delta\rho_{\rm exp}\}_{2n}=\rho_o\frac{1+n^2}{1-n^2}\frac{\Delta\omega_{n,\rm exp}}{\omega_{on}}{\rm e}^{2{\rm i}\varphi_{n,\rm exp}},\quad n\in\mathscr{N}. \tag{49}$$

Accordingly, any continuous mass distribution $\delta\rho_{\rm exp}(\theta)$ whose Fourier coefficients $\{\delta\rho_{\rm exp}\}_{2n}$, $n\in\mathscr{N}$, are given by Eq. (49), produces the measured modal mistuning $\Delta\omega_{n,\rm exp}$ and phase orientation $\varphi_{n,\rm exp}$, $n\in\mathscr{N}$, when applied to the reference ring $\mathscr{R}_{\rm ref}$. This suggests to model the real imperfect ring as a ring $\mathscr{R}_{\rm mod}$, constituted by the reference ring $\mathscr{R}_{\rm ref}$ with any such continuous mass distribution $\delta\rho_{\rm exp}(\theta)$ applied. According to Eq. (25), it turns out that the eigenfrequency $\omega_{on}$ of $\mathscr{R}_{\rm ref}$ coincides with the average of the eigenfrequencies $\omega_{n,0}$ and $\omega_{n,1}$ of $\mathscr{R}_{\rm mod}$, provided that $\delta\rho_{\rm exp}(\theta)$ is chosen with null average (i.e., $\{\delta\rho_{\rm exp}\}_0=0$). As a consequence, $\omega_{on}$ could be identified with the average of the experimentally measured eigenfrequencies.

The modes $n\in\mathscr{N}$ of the ring $\mathscr{R}_{\rm mod}$ can be trimmed, according to the linear model presented in Section 3.2, by simply adding to $\mathscr{R}_{\rm mod}$ *any* continuous mass distribution $\delta\rho_{\rm tr}(\theta)$, even different from $-\delta\rho_{\rm exp}(\theta)$, provided that its Fourier coefficients $\{\delta\rho_{\rm tr}\}_{2n}$, $n\in\mathscr{N}$, are *the opposite* of $\{\delta\rho_{\rm exp}\}_{2n}$, given by Eq. (49). This suggests that such a mass distribution $\delta\rho_{\rm tr}(\theta)$ could trim also the real imperfect ring.

As a first example, $\delta\rho_{\mathrm{tr}}(\theta)$ could be chosen such that its Fourier coefficients different from those cited above is zero: accordingly, such a continuous distribution is

$$\delta\rho_{\mathrm{tr}}(\theta) = -\sum_{n\in\mathscr{N}} 2\rho_o \frac{1+n^2}{1-n^2}\frac{\Delta\omega_{n,\mathrm{exp}}}{\omega_{on}}\cos 2(n\theta+\varphi_{n,\mathrm{exp}}). \tag{50}$$

Such a distribution is interesting, since it does not affect the eigenmodes $n\neq\mathscr{N}$. Moreover, the total mass to be added or removed from the ring vanishes. The distribution (50) is a continuous one: hence, it would require a continuous laser ablation (not to mention the difficulty arising in the region where $\delta\rho_{\mathrm{tr}}(\theta)$ is positive, requiring, e.g., a preliminary mass deposition, followed by a subsequent laser ablation).

However, among the infinitely many mass distributions $\delta\rho_{\mathrm{tr}}(\theta)$ whose Fourier coefficients are the opposite of those given by Eq. (49), there exist distributions comprised only by Dirac delta functions, which, on a physical ground, correspond to point masses to be added or removed from the ring. An easy way to obtain such distributions is to sample the function $\delta\rho_{\mathrm{tr}}(\theta)$ given in Eq. (50) at $N$ equi-spaced locations: i.e., at the angles

$$\theta_{l,\mathrm{tr}} = \theta_o + l\theta_s, \quad l = 0\ldots N-1, \tag{51}$$

where $\theta_o$ is an arbitrary initial sampling angle and $\theta_s = 2\pi/N$ is the angular sampling period. Setting $n_{\max} = \max\mathscr{N}$, and observing that the spectrum of the function $\delta\rho_{\mathrm{tr}}(\theta)$ contains spatial circular frequencies up to $2n_{\max}$, according to the Nyquist theorem, it must result:

$$\frac{2\pi}{\theta_s} = N > 2(2n_{\max}) = 4n_{\max}. \tag{52}$$

Accordingly, the continuous mass distribution given in Eq. (50) is replaced by the sampled one:

$$\delta\rho_{\mathrm{tr,s}}(\theta) = \frac{2\pi}{N}\sum_{l=0}^{N-1}\delta\rho_{\mathrm{tr}}(\theta_{l,\mathrm{tr}})\boldsymbol{\delta}_{\theta_{l,\mathrm{tr}}}(\theta). \tag{53}$$

Indeed, the distributions $\delta\rho_{\mathrm{tr}}$ and $\delta\rho_{\mathrm{tr,s}}$ have the same Fourier coefficients, up to the order $2n_{\max}$:

$$\{\delta\rho_{\mathrm{tr,s}}\}_k = \{\delta\rho_{\mathrm{tr}}\}_k, \quad |k|\leqslant 2n_{\max}, \tag{54}$$

as it is well known. However, for the sake of completeness, a direct proof is here reported. One computes:

$$\begin{aligned}\{\delta\rho_{\mathrm{tr,s}}\}_k &= \frac{1}{2\pi}\int_0^{2\pi}\delta\rho_{\mathrm{tr,s}}(\theta)\mathrm{e}^{-\mathrm{i}k\theta}\,\mathrm{d}\theta = \frac{1}{N}\int_0^{2\pi}\sum_{l=0}^{N-1}\delta\rho_{\mathrm{tr}}(\theta_{l,\mathrm{tr}})\boldsymbol{\delta}_{\theta_{l,\mathrm{tr}}}(\theta)\mathrm{e}^{-\mathrm{i}k\theta}\,\mathrm{d}\theta\\ &= \frac{1}{N}\sum_{l=0}^{N-1}\sum_{p=-\infty}^{+\infty}\{\delta\rho_{\mathrm{tr}}\}_p\mathrm{e}^{\mathrm{i}p\theta_{l,\mathrm{tr}}}\mathrm{e}^{-\mathrm{i}k\theta_{l,\mathrm{tr}}} = \sum_{p=-\infty}^{+\infty}\{\delta\rho_{\mathrm{tr}}\}_p\mathrm{e}^{\mathrm{i}(p-k)\theta_o}\frac{1}{N}\sum_{l=0}^{N-1}\mathrm{e}^{2\pi\mathrm{i}(p-k)l/N}.\end{aligned} \tag{55}$$

Recalling that $\{\delta\rho_{\mathrm{tr}}\}_p$ vanishes for $|p|>2n_{\max}$ and using Eq. (52) and the well-known identity:

$$\frac{1}{N}\sum_{l=0}^{N-1}\mathrm{e}^{2\pi\mathrm{i}ql/N} = \begin{cases}1 & \text{if } N \text{ divides } q,\\ 0 & \text{if } N \text{ does not divide } q,\end{cases} \tag{56}$$

Eq. (55) yields Eq. (54): indeed, if $\{\delta\rho_{\mathrm{tr}}\}_p$ is nonzero, then $|p|\leqslant 2n_{\max}$ and hence $|p-k|\leqslant 4n_{\max}$, so that $N$ divides $|p-k|$ only when $p=k$.

The sampled mass distribution given in Eq. (53) corresponds to the following trimming masses:

$$m_{l,\mathrm{tr}} = \frac{2\pi R}{N}\delta\rho_{\mathrm{tr}}(\theta_{l,\mathrm{tr}}), \quad l = 0\ldots N-1, \tag{57}$$

which recalling Eq. (50), can be calculated via the following explicit formula:

$$m_{l,\mathrm{tr}} = -\frac{2M_o}{N}\sum_{n\in\mathscr{N}}\frac{1+n^2}{1-n^2}\frac{\Delta\omega_{n,\mathrm{exp}}}{\omega_{on}}\cos 2(n\theta_{l,\mathrm{tr}}+\varphi_{n,\mathrm{exp}}), \quad l = 0\ldots N-1. \tag{58}$$

Of course, trimming using the above masses, located at positions $\theta_{l,\mathrm{tr}}$, would alter any trimming or splitting condition prevailing on the eigenmodes $n > n_{\max}$.

In some applications the number $N$ of trimming masses given by Eq. (52) may be too high. However, it is possible to achieve a trimming even using fewer masses, provided that:

$$\begin{aligned} &N \text{ does not divide } 4n, \ \forall n \in \mathcal{N}, \quad \text{and} \\ &N \text{ does not divide } 2n \pm 2m, \quad \forall n, m \in \mathcal{N}, n \neq m. \end{aligned} \tag{59}$$

Condition (59) was derived in Ref. [12] in the particular situations of single-mode or dual-mode trimming. It is shown here that it has a general validity, since it suffices to achieve a trimming on any arbitrary number of modes.

To this end, it is observed that condition (54) can be replaced by the following weaker condition:

$$\{\delta\rho_{\mathrm{tr,s}}\}_k = \{\delta\rho_{\mathrm{tr}}\}_k, \quad \pm k \in 2\mathcal{N}. \tag{60}$$

Moreover, reasoning as in Eq. (55), and using Eq. (56), it turns out that:

$$\{\delta\rho_{\mathrm{tr,s}}\}_k = \sum_{r=-\infty}^{+\infty} \{\delta\rho_{\mathrm{tr}}\}_{k+rN} \mathrm{e}^{\mathrm{i}rN\theta_o}. \tag{61}$$

Recalling that the base spectrum $\{\delta\rho_{\mathrm{tr}}\}_p$ is different from zero only for $\pm p \in 2\mathcal{N}$, condition (59) implies that for $\pm k \in 2\mathcal{N}$ the only nonvanishing contribution to the sum over $r$ in Eq. (61) is due to $r = 0$. Hence Eq. (60) holds and the trimming is achieved.

In passing, it is here observed that a target trimming [12], i.e., the choice of the eigenfrequency $\omega_{\overline{n}}$ of one trimmed eigenmode $\overline{n} \in \mathcal{N}$ can be easily achieved. Indeed, according to Eq. (25), it suffices to add the constant term

$$-2\rho_o\left(\frac{\omega_{\overline{n}}}{\omega_{on}} - 1\right) \tag{62}$$

to the right-hand side of Eq. (50), which amounts to increase each of the trimming masses $m_{l,\mathrm{tr}}$ given in Eq. (58) by the quantity:

$$-\frac{2M_o}{N}\left(\frac{\omega_{\overline{n}}}{\omega_{on}} - 1\right). \tag{63}$$

On the other hand, if no target trimming is required, an arbitrary constant term may be added to the right-hand side of Eq. (50), i.e. each trimming mass $m_{l,\mathrm{tr}}$ may be increased (or decreased) by the same arbitrary quantity, without modifying the achieved trimming condition. This freedom may be used, e.g., to have all the trimming masses positive (or negative), if this situation is preferred for easiness of manufacturing.

In order to validate the proposed trimming procedure, the imperfect ring described in case (iii) of Section 5 is here considered. Eigenmodes $n = 2$ and 3 are trimmed by using $N = 13$ or $N = 7$ equispaced trimming masses, located at positions $2l\pi/N$, $l = 0 \ldots N-1$. The required trimming masses are computed through the explicit formula (58) and are reported in Table 9. The outcome of the trimming procedure is reported in Table 10, where the trimmed eigenfrequencies, which are degenerate according to the LT model, are compared

Table 9
Outcome of the trimming procedure based on LT and FT [11,12] models, applied to the imperfect ring of case (iii): trimming masses [$10^{-2}$ kg]

| Theory | # | $m_1$ | $m_2$ | $m_3$ | $m_4$ | $m_5$ | $m_6$ | $m_7$ | $m_8$ | $m_9$ | $m_{10}$ | $m_{11}$ | $m_{12}$ | $m_{13}$ |
|---|---|---|---|---|---|---|---|---|---|---|---|---|---|---|
| LT | 13 | −5.18 | 3.08 | 2.20 | −5.94 | 5.33 | −2.98 | 3.46 | −7.28 | 10.2 | −8.64 | 4.30 | −1.98 | 3.44 |
| LT | 7 | −9.62 | 10.6 | 11.9 | 7.67 | 2.42 | −16.6 | −6.31 | | | | | | |
| FT [12] | 7 | −20.6 | 19.6 | 28.5 | 0.9 | −1.5 | 1.5 | −0.9 | | | | | | |
| FT [11] | 2 | −52.3 | −39.8 | | | | | | | | | | | |

Trimmed eigenmodes $n = 2, 3$. Different number of masses considered.

Table 10
Outcome of the trimming procedure based on LT and FT [11,12] models, applied to the imperfect ring of case (iii): trimmed eigenfrequencies (Hz)

| Theory | # masses | $n=2$ | | $n=3$ | |
|---|---|---|---|---|---|
| LT | 13 | 35.373 | | 100.05 | |
| RR check | | 35.417 | 35.441 | 100.09 | 100.20 |
| Residual mistuning | | 0.068% | | 0.115% | |
| LT | 7 | 35.373 | | 100.05 | |
| RR check | | 35.491 | 35.542 | 100.19 | 100.77 |
| Residual mistuning | | 0.144% | | 0.579% | |
| FT [12] | 7 | 34.781 | | 98.375 | |
| RR check | | 34.897 | 34.950 | 98.484 | 99.179 |
| Residual mistuning | | 0.152% | | 0.706% | |
| FT [11] | 2 | 37.602 | | 106.36 | |
| RR check | | 37.638 | 37.709 | 106.16 | 107.13 |
| Residual mistuning | | 0.189% | | 0.919% | |

Exact eigenfrequencies (Hz) and residual mistuning (%) computed by the RR method also reported. Trimmed eigenmodes $n=2,3$. Different number of masses considered.

to the exact eigenfrequencies supplied by the RR method. The residual percentage mistuning, defined as $|\omega_{n,1}-\omega_{n,0}|/\omega_{n,0}$, is also indicated. For the sake of comparison, results obtained in Ref. [12], Table 7 (7 equally spaced masses), and Ref. [11], Table 3 (two masses placed at $\theta_1=3.95^\circ$ and $\theta_2=144.31^\circ$), relevant to the same imperfect ring, are also reported.

The results in Table 10 show that the proposed trimming procedure based on the LT method yields satisfactory trimming conditions using both 13 and 7 trimming masses. As expected, the fewer masses are employed, the greater is the residual mistuning. Indeed, when fewer masses are used, higher values of masses are required and, as a consequence, the linear theory has a reduced accuracy in estimating the eigenfrequencies. Equivalent results are obtained by using the LT or FT models with the same number of masses. The closed-form expression (57) for the trimming masses, valid for any set of modes to be trimmed, makes especially convenient the use of the LT model.

## 7. Conclusions

The dynamical behavior of linearly elastic imperfect rings was studied in this paper. The imperfections were modeled as perturbations of the linear mass density and the in-plane bending stiffness of a perfect ring.

A linear theory and an enhanced theory were derived. The former yielded closed-form expressions for both the eigenfrequencies and the eigenmodes, and turned out to be accurate for sufficiently small imperfections. The latter turned out to be accurate even for large imperfections, but required an iterative solving procedure.

Some case-study problems of technological interest were considered, in order to validate the proposed theories against the results provided by the Ritz–Rayleigh method. The numerical examples showed that the eigenmodes of an imperfect ring may significatively deviate from a sinusoidal shape, exhibiting localization of vibration amplitude.

The proposed linear theory was applied to the trimming problem of an imperfect ring. A simple, closed-form expression was presented for computing the masses, to be placed at equispaced positions, able to trim any selected number of eigenmodes. The quality of the achieved trimming was tested by evaluating, via the Ritz–Rayleigh method, the residual mistuning between the trimmed eigenfrequencies. Finally, a rule found in Ref. [12] concerning invalid combinations of masses and modes for single- or dual-mode trimming, was generalized to the multi-mode trimming case.

## Acknowledgments

The authors wish to thank Professor Franco Maceri for his valuable comments on this paper. This work was partially supported by CNR/MIUR Grant No. CU07.00008 ST/97.

## References

[1] A.K. Rourke, S. McWilliam, C.H.J. Fox, Frequency trimming of a vibrating ring-based multi-axis rate sensor, *Journal of Sound and Vibration* 280 (2005) 495–530.
[2] B.J. Gallacher, J. Hedley, J.S. Burdess, A.J. Harris, A. Rickard, D.O. King, Electrostatic correction of structural imperfections present in a microring gyroscope, *Journal of Microelectromechanical Systems* 14 (2) (2005) 221–234.
[3] J. Tang, K.W. Wang, Vibration delocalization of nearly periodic structures using coupled piezoelectric networks, *ASME Journal of Vibration and Acoustics* 125 (2003) 95–108.
[4] X. Fang, J. Tang, E. Jordan, K.D. Murphy, Crack induced vibration localization in simplified bladed-disk structures, *Journal of Sound and Vibration* 291 (2006) 395–418.
[5] C.H.J. Fox, A simple theory for the analysis and correction of frequency splitting in slightly imperfect rings, *Journal of Sound and Vibration* 142 (2) (1990) 227–243.
[6] R.S. Wang, C.H.J. Fox, S. McWilliam, The in-plane vibration of thin rings with in-plane profile variations, part I: general background and theoretical formulation, *Journal of Sound and Vibration* 220 (3) (1999) 497–516.
[7] P.A.A. Laura, C.P. Filipich, R.E. Rossi, J.A. Reyes, Vibrations of rings of variable cross section, *Applied Acoustics* 25 (1988) 225–234.
[8] S. McWilliam, J. Ong, C.H.J. Fox, On the statistics of natural frequency splitting for rings with random mass imperfections, *Journal of Sound and Vibration* 279 (2005) 453–470.
[9] R. Eley, C.H.J. Fox, S. McWilliam, Anisotropy effects on the vibrations of circular rings made from crystalline silicon, *Journal of Sound and Vibration* 228 (1) (1999) 11–35.
[10] M. Esmaeili, M. Durali, N. Jalili, Ring microgyroscope modeling and performance evaluation, *Journal of Vibration and Control* 12 (5) (2006) 537–553.
[11] A.K. Rourke, S. McWilliam, C.H.J. Fox, Multi-mode trimming of imperfect rings, *Journal of Sound and Vibration* 248 (4) (2001) 695–724.
[12] A.K. Rourke, S. McWilliam, C.H.J. Fox, Multi-mode trimming of imperfect thin rings using masses at pre-selected locations, *Journal of Sound and Vibration* 256 (2) (2002) 319–345.